





Article

Towards a High-Affinity Peptidomimetic Targeting Proliferating Cell Nuclear Antigen from *Aspergillus fumigatus*

Bethiney C. Vandborg^{1,2} , Aimee J. Horsfall^{1,3} , Jordan L. Pederick^{1,2} , Andrew D. Abell^{1,3}
and John B. Bruning^{1,2,*} 

- ¹ Institute of Photonics and Advanced Sensing (IPAS), The University of Adelaide, Adelaide 5005, Australia; bethiney.vandborg@adelaide.edu.au (B.C.V.); jordan.pederick@adelaide.edu.au (J.L.P.); andrew.abell@adelaide.edu.au (A.D.A.)
² School of Biological Sciences, The University of Adelaide, Adelaide 5005, Australia
³ ARC Centre of Excellence for Nanoscale BioPhotonics, The University of Adelaide, Adelaide 5005, Australia
* Correspondence: john.bruning@adelaide.edu.au

Abstract: Invasive fungal infections (IFIs) are prevalent in immunocompromised patients. Due to alarming levels of increasing resistance in clinical settings, new drugs targeting the major fungal pathogen *Aspergillus fumigatus* are required. Attractive drug targets are those involved in essential processes like DNA replication, such as proliferating cell nuclear antigens (PCNAs). PCNA has been previously studied in cancer research and presents a viable target for antifungals. Human PCNA interacts with the p21 protein, outcompeting binding proteins to halt DNA replication. The affinity of p21 for hPCNA has been shown to outcompete other associating proteins, presenting an attractive scaffold for peptidomimetic design. p21 has no *A. fumigatus* homolog to our knowledge, yet our group has previously demonstrated that human p21 can interact with *A. fumigatus* PCNA (afumPCNA). This suggests that a p21-based inhibitor could be designed to outcompete the native binding partners of afumPCNA to inhibit fungal growth. Here, we present an investigation of extensive structure–activity relationships between designed p21-based peptides and afumPCNA and the first crystal structure of a p21 peptide bound to afumPCNA, demonstrating that the *A. fumigatus* replication model uses a PIP-box sequence as the method for binding to afumPCNA. These results inform the new optimized secondary structure design of a potential peptidomimetic inhibitor of afumPCNA.



Citation: Vandborg, B.C.; Horsfall, A.J.; Pederick, J.L.; Abell, A.D.; Bruning, J.B. Towards a High-Affinity Peptidomimetic Targeting Proliferating Cell Nuclear Antigen from *Aspergillus fumigatus*. *J. Fungi* **2023**, *9*, 1098. <https://doi.org/10.3390/jof9111098>

Academic Editor: Gill Diamond

Received: 11 October 2023
Revised: 4 November 2023
Accepted: 7 November 2023
Published: 10 November 2023



Copyright: © 2023 by the authors. Licensee MDPI, Basel, Switzerland. This article is an open access article distributed under the terms and conditions of the Creative Commons Attribution (CC BY) license (<https://creativecommons.org/licenses/by/4.0/>).

Keywords: PCNA; DNA replication proteins; non-tag purification; peptide characterization; *Aspergillus fumigatus*; X-ray crystallography

1. Introduction

Invasive fungal infections (IFIs) are a prevalent cause of death in immunocompromised patients [1]. A major fungal pathogen causing such infections is *Aspergillus fumigatus*, a filamentous fungus that is usually present in decaying organic matter [2,3]. The conidia of *A. fumigatus* inhaled from the environment can be cleared from the lungs by a healthy immune system. However, when this fails, the conidia can reach the lower airways and evade host immune cells [4]. This can result in the infection of the bronchi and sinuses and dissemination to the brain and other vital organs through the circulatory system [5,6]. This is known as invasive aspergillosis. When invasive aspergillosis invades the nervous system, it has mortality rates of up to 90% [7].

As the infection rates of *A. fumigatus* increase, more species and therefore differing antifungal resistances arise, which have been associated with negative clinical outcomes [8]. Although many antifungals are available, the mortality rates remain high due to the development of drug resistance in *A. fumigatus* [9]. Current treatments of invasive aspergillosis target the components of the cell membrane: for example, the antifungal amphotericin B [10]. Unfortunately, in addition to increasing resistance rates, amphotericin B is associated with severe side effects, the most notable being kidney and liver toxicity [11]. There

has been increasing resistance to the antifungal triazole reported via unknown resistance mutations [12]. As such, there is an urgent need for improved diagnostic protocols and a broader range of antifungal options [13].

The DNA replication process is a desirable target for an antifungal product; hence, *A. fumigatus* proliferating cell nuclear antigen (afumPCNA) has been hypothesised as a fungal target for the development of new antifungals [14]. The PCNA processivity factor is also known as the sliding clamp, as DNA slides through its central cavity. PCNA functions as a docking platform to allow DNA polymerases and a host of DNA replication and repair machinery to interact at the replication fork [15]. PCNA has been proposed as a target for the treatment of multiple diseases as it is essential for cell replication, and its absence has been shown to cause embryonic lethality [16,17].

The X-ray crystal structure of apo afumPCNA solved at 2.6 Å resolution [14] shows a trimeric tertiary structure that is similar to that of hPCNA by the superimposition of the structures (PDB: 8GJF and PDB: 7KQ1), this revealed a root-square standard deviation (RMSD) of 0.939 Å. Despite this, the proteins only have a sequence similarity of 53% [14]. The PCNA homotrimer comprises two domains, with each containing two alpha helices and nine beta strands (Figure 1b), connected by a motif known as the interdomain connecting loop (IDCL), which forms part of the PCNA surface with which binding domain proteins interact. The negatively charged beta sheets allow interactions with replication and repair proteins, and the positively charged alpha helices allow non-specific interactions with double-stranded DNA on the inside of the sliding clamp (Figure 1a). It has been hypothesised that the difference in amino acid sequences present at the surface of PCNA, to which interacting partners bind, could allow for the specificity of afumPCNA over hPCNA in the design of a fungal replication inhibitor [14]. This illustrates the importance of investigating the structure of afumPCNA to understand how interacting peptides bind in aiding rational drug design.

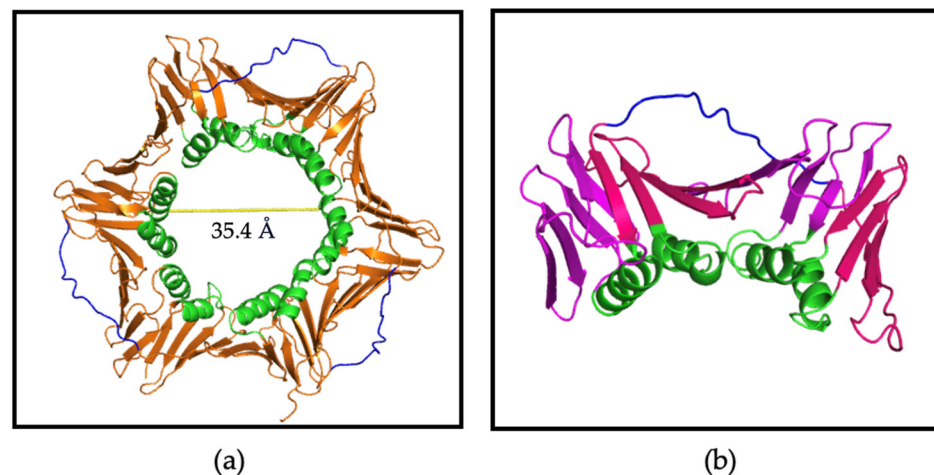


Figure 1. PCNA homotrimer structure (PDB:7KQ0) [18]. (a) Trimer: PCNA surface shown in orange, IDCL shown in blue, and positively charged alpha helices shown in green. Central cavity is 35.4 Å wide. (b) Monomer: beta sheets shown in magenta and pink, alpha helices shown in green, and IDCL shown in blue. Made using Pymol Version 1.2 [19].

In an effort to target PCNA, the most thoroughly characterised peptide inhibitor is derived from the tumour suppressor protein p21. Protein p21 (also known as cyclin-dependent kinase inhibitor 1), a cyclin-dependent kinase inhibitor, binds hPCNA to outcompete binding partners in order to halt DNA replication for repair systems [20], thus regulating the cell cycle during DNA damage. The affinity of peptides derived from p21 binding to hPCNA has been shown to be much higher than other associating proteins [18,21]. PCNA-interacting proteins, including p21, are allowed access to DNA by interacting with PCNA via the PCNA-interacting protein (PIP) box sequence, $Q_{144}X_{145}X_{146}\Phi_{147}X_{148}X_{149}\Psi_{150}\Psi_{151}$,

a consensus sequence in which the glutamine residue (Gln₁₄₄) binds the ‘Q pocket’ of the PCNA hydrophobic patch, Φ_{147} represents a hydrophobic residue, and Ψ_{150} and Ψ_{151} represent aromatic residues. The sequence and affinity of the PIP-box are theorised to correlate with the protein’s function [22]. The combination of the hydrophobic residue and two aromatic residues forms a hydrophobic plug that inserts into the PCNA surface and twists the peptide’s backbone from residues 147 to 151 into a 3_{10} helix that is conserved between binding partners. This secondary structure is critical for high-affinity binding. Other interactions that increase affinity are the ionic charged interactions of the C-terminal flank of the PIP-box with the surface of PCNA, and the N-terminal flank of the PIP-box creates an antiparallel β -sheet with the C-terminus of PCNA.

The fluorescence polarisation experiments of afumPCNA and a 22 amino acid peptide derived from the C-terminus of (human) p21 containing the PIP-box (139–160) have demonstrated their interaction, suggesting that afumPCNA interacts with DNA binding proteins using a similar PIP-box mechanism compared to the human system [14]. Given that *Aspergillus fumigatus* does not have a known p21 equivalent and this p21-derived peptide shows high-affinity interactions, further investigation into human PIP-box sequence interactions with afumPCNA may indicate the characteristics of a high-affinity mimetic. The p21 scaffold may serve as a useful starting point for designing the peptide inhibitors of afumPCNA. This also suggests that an artificial PIP-box could be designed specifically to disrupt the function of afumPCNA and highlights afumPCNA as a potential drug target for treating fungal infections. Fungal PCNA-interacting proteins were investigated as a means of probing these unknown PIP-box sequences; therefore, they can uncover interactions that could be advantageous to a mimetic. These PIP-box candidates were investigated in fungal proteins DNA polymerase (DNAPol), DNA ligase (DNALig), flap endonuclease 1 (FEN1), and replication factor C (RFC).

Here, we present the first structure of a PIP-box peptide bound to afumPCNA and characterise the interactions of afumPCNA with predicted fungal protein PIP-box candidates. Via binding affinity assays and X-ray crystallography studies, the findings support the hypothesis that the fungal replication model uses a PIP-box sequence as the method for binding to fungal PCNA, and a rational design for a potential peptidomimetic is presented.

2. Materials and Methods

2.1. Peptides

The following peptides were obtained and synthesised by Genscript Biotech, Singapore at a purity of >95%, and they were purified via HPLC. Peptides denoted with * were designed by B. Vandborg. The sequences are shown in bold.

5FAM-p21-22mer (5FAM)-**GRKRRQTSMTDFYHSKRRLIFS**

p21 μ p21 μ -15mer **KRRQTSMTDFYHSKR**

p21 μ -afumDNALIG **KRRQRVRSIASFFHSKR***

p21 μ -afumDNAPOL **KRRQKELSRFDHFSK***

p21 μ -afumFEN1 **KRRQSRLEGFFHSKR***

p21 μ -afumRFC **KRRMPTDIRNFFHSKR***

The following peptides were synthesised by Fmoc SPPS, as described below in Section 2.1.1; each has a C terminal carboxyl amide. The sequences are shown in bold.

p21 μ (p21 μ -15mer) **KRRQTSMTDFYHSKR**

p21 μ -RD2 **KRRQTRITEYFHSKR**

p21 μ -Q144M **KRRMTSMTDFYHSKR**

p21 μ -T145K **KRRQKSMTDFYHSKR**

p21 μ -T145D **KRRQDSMTDFYHSKR**

p21 μ -S146R **KRRQTRMTDFYHSKR**

p21 μ -M147L **KRRQTSMTDFYHSKR**

p21 μ -M147I **KRRQTSITDFYHSKR**

p21 μ -D149E **KRRQTSMTDFYHSKR**

p21 μ -F150Y **KRRQTSMTDYHSKR**

p21 μ -Y151F **KRRQTSMTDFFHSKR**
p21 μ -FY150151YF **KRRQTSMTDYFHSKR**

2.1.1. Peptide Synthesis by Fmoc SPPS

All peptides were prepared on Rink Amide functionalized polystyrene resin (Agilent, Santa Clara, CA, USA) and synthesized via Fmoc/*t*Bu solid-phase peptide synthesis (SPPS), as previously described [18]. The peptides were purified via semi-preparatory RP-HPLC, and the purity and identity were confirmed via analytical HPLC and MS, as previously reported [18].

2.2. Expression of Recombinant *afumPCNA*

A. fumigatus PCNA was expressed as described in Vandborg 2023 [23].

A glycerol stock of *E. coli* BL21 (DE3) cells carrying a codon-optimized *afumPCNA*-pMCSG19 plasmid was grown in a 100 mL overnight culture. Two 1 L baffled flasks containing LB with 100 μ g/mL of ampicillin were inoculated with 50 mL of the overnight culture. Cultures were incubated at 37 °C until OD₆₀₀ = 0.7, and expression was induced with a final concentration of 0.5 mM IPTG. Cultures were grown overnight at 16 °C and shaking occurred at 200 rpm. Cultures were pelleted at 5000 \times g for 20 min. After removing the supernatant, pellets were resuspended in 20 mL 20 mM Tris-HCl pH 7.5, 20 mM NaCl, and 2 mM DTT and then lysed via sonication at 70% amplification for 20 s with a 40 s waiting period for 25 cycles. Lysate was clarified via pelleting at 45,000 \times g for 45 min, and the supernatant was collected for purification.

2.3. Purification of Recombinant *afumPCNA*

A. fumigatus PCNA was purified as described in Vandborg 2023 [23].

Buffer solutions were filtered before being used. Clarified lysate containing *afumPCNA* was first purified at 4 °C via fast protein liquid chromatography (FPLC) using anion exchange chromatography and two DEAE columns in series (HiTrap DEAE FF 5 mL column). They were then equilibrated in Buffer A (20 mM Tris-HCl pH 7.5, 20 mM NaCl, 2 mM DTT), and *afumPCNA* was eluted using a linear gradient (0.02 M–0.7 M NaCl). Fractions containing *afumPCNA* were pooled, and ammonium sulphate was added dropwise to a final concentration of 1.5 M from a stock solution of 3 M ammonium sulphate. The sample was allowed to stir gently for 1 h at 4 °C to allow DNA–protein dissociation, and then it was applied to hydrophobic interaction chromatography (HiTrap Phenyl FF (high sub) 5 mL column) and equilibrated in Buffer B (20 mM Tris-HCl pH 7.5, 20 mM NaCl, 2 mM DTT, 0.5 mM EDTA, 1.5 M ammonium sulphate) and eluted in Buffer C (20 mM Tris-HCl pH 7.5, 2 mM DTT, and 0.5 mM EDTA) with a reverse linear gradient (1.5 M–0 M ammonium sulphate). Fractions containing *afumPCNA* were pooled and dialyzed overnight in Buffer A. *afumPCNA* was then applied to a second anion exchange step. The Q Sepharose column (5 mL Q Sepharose FF column (GE)) was equilibrated in Buffer A, and the protein was eluted using a linear gradient (0.02 M–0.7 M NaCl). Fractions containing *afumPCNA* were pooled and dialyzed overnight in 20 mM Tris-HCl pH 7.5, 10% *v/v* glycerol, 2 mM DTT, and 0.5 mM EDTA. The protein for crystallography was concentrated to ~10 mg/mL using a centrifugal filter unit (50 kDa molecular mass cut off) and stored at –80 °C.

2.4. Surface Plasmon Resonance Protocol

Surface plasmon resonance (SPR) experiments were performed as previously described [18]. The running buffer used for ligand attachment and analyte-binding experiments was a 10 mM HEPES buffer with 150 mM NaCl, 3 mM EDTA, and 0.05% Tween-20, adjusted to pH 7.4 with 2 M NaOH. A GE CM5 (series S) sensor chip was primed with the running buffer and pre-conditioned with successive injections (2 \times 50 s, 30 μ L/min) of 50 mM NaOH, 10 mM HCl, 0.1% SDS, 0.85% H₃PO₄, and 50 mM glycine pH 9.5, respectively. The surface was then activated with an injection of 0.2 M 1-ethyl-3-(3-dimethylaminopropyl)carbodiimide (EDC) and 50 mM N-hydroxysuccinimide (NHS) (600 s, 10 μ L/min). *A. fumigatus* PCNA (5 μ L,

12 mg/mL) was diluted into the running buffer (245 µL). Upon the preactivation of the surface, the protein was further diluted to a final concentration of 25 µg/mL in 10 mM NaAc (~pH 4.6). This solution was immediately injected over the target flow cell (10 µL/min) to immobilize ~1500 RU. Both the target and reference flow cells were then blocked with 1.0 M ethanolamine at pH 8.5 (600 s, 10 µL/min). The chip was left to stabilize before sample injections commenced.

Peptide stock solutions for use in SPR experiments were prepared in MilliQ water. The peptide stock concentration was determined via 205 nm absorbance with NanoDrop2000. The ε₂₀₅ for each peptide was calculated using an online calculator (<http://nickanthis.com/tools/a205.html>, accessed on 22 August 2022 [24]); however, additional glycine residue was added to each peptide sequence to account for the terminal amide of the peptides synthesized in-house. The peptide stock solution’s concentration was then calculated using Beer’s Law.

Steady-state affinity experiments were conducted at a flow rate of 30 µL/min, with a starting contact time of 40 s and dissociation of 30 s. A 2-fold serial dilution was performed for each peptide, with 8 samples injected sequentially from the lowest to highest concentrations; they were preceded by a buffer-only blank injection. After each injection, the surface was regenerated with 2 M NaCl (2 × 30 s, 25 µL/min). All data were analyzed using the GE Biosystems Biacore S200 Evaluation Software, Version 1.0 (Build: 20). All data are summarized in Table 1.

Table 1. p21 Peptide SPR data against afumPCNA in comparison to human PCNA binding affinity as shown in Horsfall 2021 [18]. K_D is the affinity constant. SD, standard deviation. All peptides are C-terminally amidated. Changes to the p21µ scaffold are indicated in bold. The PIP-box residues are separated from flanking residues with spaces. Conserved PIP positions are underlined. More information can be found in Table S1 and Figure S1.

Name	Sequence	afumPCNA Binding Affinity K _D (nM) ± SD (nM)	Human PCNA Binding Affinity K _D (nM) ± SD (nM) [18]
p21(139–160)	¹³⁹ GRKRR <u>Q</u> TSM <u>T</u> DFY HSKRRLIFS ¹⁶⁰	69.7 ± 20.2	4.3 ± 1.3
p21µ	¹⁴¹ KRR <u>Q</u> TSM <u>T</u> DFY HSKR ¹⁵⁵	265.1 ± 5.9	12.3 ± 0.5
p21µ-RD2	¹⁴¹ KRR <u>Q</u> TRITE <u>Y</u> F HSKR ¹⁵⁵	20.3 ± 6.8	1.1 ± 0.3
p21µ-Q144M	¹⁴¹ KRR <u>M</u> TSM <u>T</u> DFY HSKR ¹⁵⁵	41,400 ± 0.8	1544 ± 159
p21µ-T145K	¹⁴¹ KRR <u>Q</u> KSM <u>T</u> DFY HSKR ¹⁵⁵	10,000 ± 0.7	98 ± 10.8
p21µ-T145D	¹⁴¹ KRR <u>Q</u> DSM <u>T</u> DFY HSKR ¹⁵⁵	4100 ± 0.31	714 ± 30.4
p21µ-S146R	¹⁴¹ KRR <u>Q</u> TRM <u>T</u> DFY HSKR ¹⁵⁵	64.4 ± 18.4	4.3 ± 1.3
p21µ-M147L	¹⁴¹ KRR <u>Q</u> TS <u>L</u> TDFY HSKR ¹⁵⁵	382 ± 51.0	20.5 ± 1.7
p21µ-M147I	¹⁴¹ KRR <u>Q</u> TSITDFY HSKR ¹⁵⁵	37.1 ± 7.8	11.1 ± 0.3
p21µ-D149E	¹⁴¹ KRR <u>Q</u> TSMTEFY HSKR ¹⁵⁵	400.7 ± 45.6	12.7 ± 1.4
p21µ-F150Y	¹⁴¹ KRR <u>Q</u> TSMTD <u>Y</u> Y HSKR ¹⁵⁵	75.2 ± 18.9	20.2 ± 0.4
p21µ-Y151F	¹⁴¹ KRR <u>Q</u> TSMTDFF HSKR ¹⁵⁵	167.2 ± 19.1	10.6 ± 1.5
p21µ-FY150151YF	¹⁴¹ KRR <u>Q</u> TSMTD <u>Y</u> F HSKR ¹⁵⁵	96.4 ± 19.6	2.2 ± 0.5

2.5. Protein-Peptide Co-Crystallization Experiments

To form the protein–peptide complex, afumPCNA was mixed with the peptide of interest at a molar ratio of 1:1.2. After incubation on ice for 30 min, the sample was pelleted at 16,000× g for 10 min to remove aggregates. Crystals were grown via the hanging drop vapor diffusion method in 24-well plates containing 500 µL of well solution by mixing 1 µL of protein and peptide with equal volumes of well solutions. The diffracting crystals of afumPCNA bound to p21µ grew in 0.2 M Tacsimate pH 4.0 0.1M Na Acetate and 16% PEG 3350 (Hampton Research Aliso Viejo, CA, USA, product code HR2-591) at 16 °C after 3 weeks (Figure S2). The diffracting crystals of afumPCNA bound with p21µ-afumRFC grew in 0.2M Tacsimate pH 4.0 0.1M Na Acetate and 16% PEG 3350 (HR2-591) in a tray

at 16 °C after 3 weeks (Figure S3). Crystals were mounted on cryo-loops, and they were cryoprotected using paratone-N and flash-cooled in liquid nitrogen. Data were collected at 100 K using the MX1 beamline at the Australian Synchrotron (Clayton, VIC, Australia). Diffraction data were indexed and integrated using XDS (X-ray Detector Software), Version January 10, 2022 [25]. Pointless (CCP4i) [26] was used to create an mtz reflection file for scaling. Data were scaled and merged using Aimless (CCP4i) [27] at a resolution of 2.0 Å for afumPCNA bound with p21 μ and 2.30 Å for afumPCNA bound with p21 μ afumRFC. The phase problem was solved via molecular replacements using Phaser MR (CCP4i) [28] and a search model (PDB: 5TUP). Solutions were refined in Phenix Refine [29,30] in iterative rounds with manual rebuilding in Coot [31] (Figures S4 and S5). Data collection and refinement statistics are summarized in Table S2. The final structures of afumPCNA bound with p21 μ and p21 μ RFC are deposited on the RCSB database under accession numbers 8GJF and 8GJ5, respectively.

2.6. Computational Modelling

The models of peptides bound to afumPCNA were constructed using the structure of afumPCNA bound with the p21 μ peptide (PDB: 8GJF) as a starting template, and the necessary, deleted, and unresolved side chains of residues were modelled into the computational structure.

The manual refinement of the computational linker was carried out in Coot [31]. Energy minimisation/annealing ($n = 30$) for refinement was carried out in ICM-Pro Molsoft [32,33]. Refined models were analysed using PyMOL Version 1.2 [19] to validate the model by comparing it against p21 μ (PDB: 8GJF) and assessing side chain interactions. The resulting structures were visualized in PyMOL [19], and they are depicted in Figures S4–S17.

3. Results

3.1. A p21 Peptide Library Interacts with afumPCNA in a Similar Trend Compared to hPCNA

The p21-derived peptide (139–160) (Table 1) [21] was previously shown to bind to afumPCNA via fluorescence polarization with a K_D of 3.1 μ M [14]. Here, we build on this observation and interrogate the binding of afumPCNA with respect to various peptides. Previously, a shorter scaffold of this 22 amino acid p21 peptide was derived and synthesized: p21 μ (141–155). It is 14 amino acids long, and it retained high-affinity binding, which was used to construct a library with variations relative to PIP-box residues [18] as a rational starting point for the investigation of the fungal binding site.

The p21 PIP-box contains a conserved glutamine residue that binds a conserved hydrophobic pocket on hPCNA; this was shown to be valuable in binding afumPCNA. The p21 glutamine residue (Gln₁₄₄), which binds the ‘Q pocket’ of the hydrophobic patch on human PCNA, forms two hydrogen bonds relative to the carbonyl backbone moieties of residues Ala₂₅₂ and Pro₂₅₃ of the PCNA main chain. These residues are conserved in the afumPCNA sequence (Figure 2); hence, as for the hPCNA investigation, the modification of Gln₁₄₄ into Met, as in p21 μ -Q144M, reduces the binding of peptide p21 μ -Q144M to afumPCNA from 265.1 nM to 41,400 nM.

The importance of residues in the non-conserved position of the PIP-box was previously shown to be important in binding to the PCNA surface in the human system [34]. To probe the effect of altering amino acids in this region of the PIP-box and its affinity to afumPCNA, the peptide was altered from Ser₁₄₆ to an Arg residue. This produced an affinity of K_D 64.4 nM, improved from the p21 μ binding affinity of K_D 265.1 nM. This was also previously observed in hPCNA, which was hypothesised to be due to an increase in side chain length [18]. The Ser to Arg variation changes the distance between residues, strengthening the intramolecular hydrogen bond to the carbonyl of Asp₁₄₉, stabilising the peptide’s 3_{10} helical structure (Figure S10). This suggests that lengthening the side chain would also improve the binding of the p21 μ -D149E peptide to afumPCNA; however, an Asp₁₄₉ modification to Glu showed reduced binding affinity with a K_D of 400.6 nM,

Table 2. Sequences of candidate fungal protein PIP-boxes in comparison to established human protein PIP-boxes. Sequences that fit the model of an eight-residue section with Q at the beginning, a hydrophobic residue in the middle, and aromatic residues at the end are shown in bold. Residues that are found to be identical between human and fungal PIP-boxes are underlined.

Protein Name	<i>Homo Sapiens</i> PIP-Box Sequence	<i>Aspergillus fumigatus</i> PIP-Box Sequence Candidates
FEN1	<u>Q</u> RLDDFF	Q <u>SR</u> LE <u>GF</u> F
RFC1	<u>M</u> DIRKFF	<u>M</u> P T <u>D</u> IR <u>N</u> F F
DNA Polymerase POLD3	<u>Q</u> V SIT <u>G</u> F F	Q <u>K</u> EL <u>S</u> R <u>F</u> D
DNA Ligase	<u>Q</u> R S <u>I</u> M S <u>F</u> F	<u>Q</u> R <u>V</u> R S <u>I</u> A S <u>F</u> F

The major differences between human and fungal PIP-boxes appear at the non-conserved residues of the canonical PIP-box sequence. In particular, in the p21 μ afumDNALig and p21 μ afumRFC sequence, additional residues were interspaced with conserved residues, possibly interfering with the alignment of the canonical structure and the contact with the protein's surface. To elaborate, the RFC1 PIP-box found in humans has the correct amount of non-conserved residues, but the candidate for *A. fumigatus* has two extra residues between the conserved methionine residue and the conserved hydrophobic residue isoleucine (Table 2).

Each *A. fumigatus* PIP-box sequence exhibits a Gln₁₄₄-conserved residue, except the RFC sequence. This significant difference between the human and fungal candidate PIP-box leads to the hypothesis that the p21 μ afumRFC peptide could not bind to afumPCNA with high affinity. However, it is surprisingly bound with <100 nM affinity.

3.3. X-ray Crystallography Study of the p21 μ Peptide Bound to afumPCNA

The first co-crystal structure of afumPCNA bound with the p21 μ scaffold peptide was solved at 2.0 Å resolution (PDB: 8GJF) in order to examine the details of the binding interaction (Figure 3). The structure shows that the overall fold of the p21 μ peptide bound to the surface of afumPCNA is similar to the structure of the p21 μ peptide bound to hPCNA (PDB: 7KQ1), as illustrated by the RMSD value of 0.939 Å. The p21 μ peptide in the afumPCNA structure (PDB: 8GJF) displays a notable charged interaction between Arg₁₄₃ and Glu₁₄₉, a 3.2 Å salt bridge interaction (Figure 4b) that was not previously shown as the extended Arg₁₄₃ side chain was not present in the hPCNA crystal structure (Figure 4a), illuminating a new interaction that also strengthens the 3_{10} helical structure.

Differences in the protein sequence of afumPCNA and hPCNA account for the shift in affinity with the conservation of the secondary structure of the peptide. There is structural conservation around the 3_{10} helical secondary structure and PIP-box, with more variability on the N- and C-terminus (Figure 4c) likely due to the mobility of the ends of the peptide and changes in IDCL residues. Previous literature interpreting the difference in the binding of p21-based peptides to afumPCNA compared to hPCNA used molecular dynamics to illustrate that the weakness of the p21 peptide (139–160) because afumPCNA came from differences in these protein binding domain residues [14]. One prominent example is residue His125, which forms an antiparallel β -sheet with the C-terminal residues of p21 peptide on hPCNA (139–160); however, in the afumPCNA structure, afumPCNA His125 obstructs the formation of a favorable side chain hydrogen bond with the His152 side chain of the p21 peptide (139–160). This has the effect of pushing the C-terminus to be quite distant from the protein's surface while not forming the hydrogen bonds of the β -sheet as observed in the human structure. There is also the loss of 3.4 Å hydrogen bond interactions between hPCNA Gln131 and the Tyr151 phenol of p21 μ in afumPCNA as this residue is Thr131.

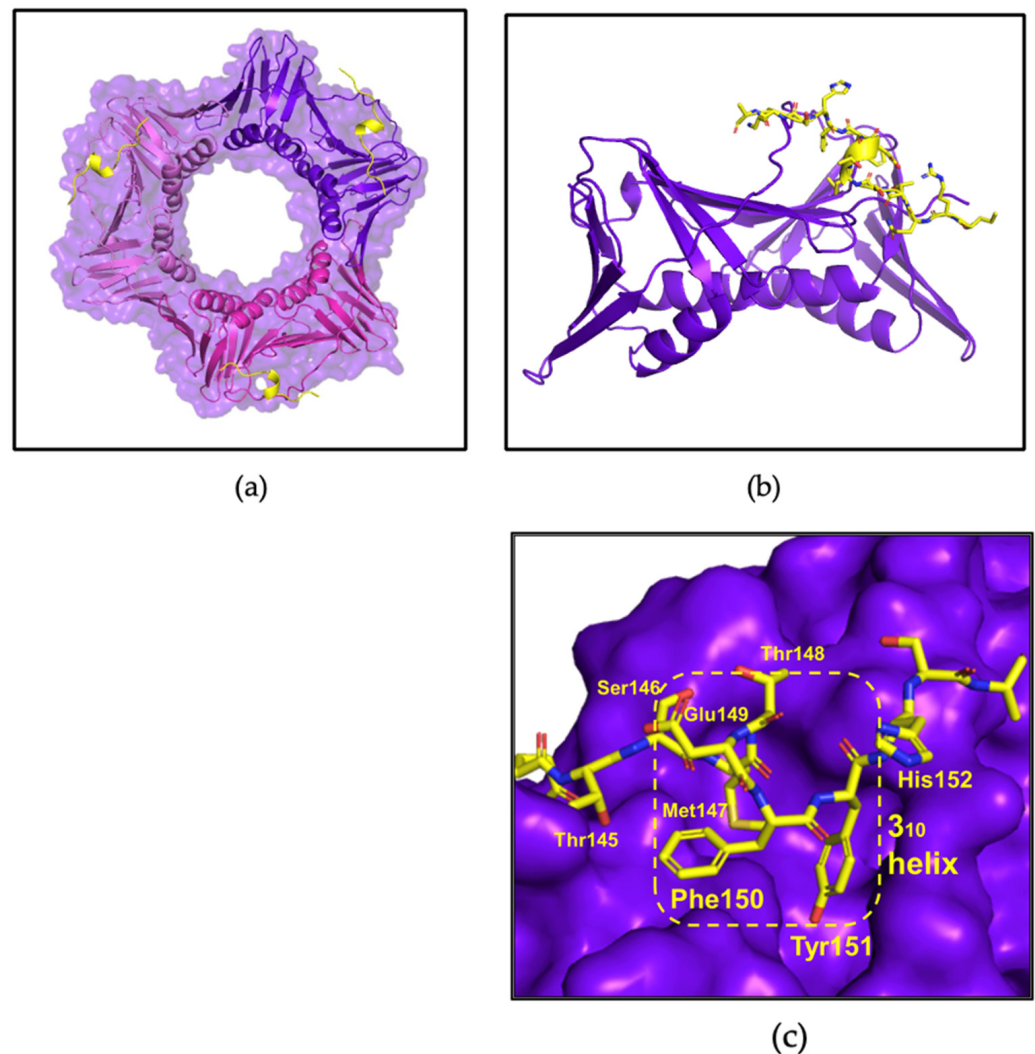


Figure 3. afumPCNA bound with p21 μ structure (PDB: 8GJF). (a) Trimer: afumPCNA surface shown in purple and p21 μ shown in olive green. (b) Monomer: afumPCNA shown in purple and p21 μ shown in olive green. (c) PIP-box binding site: 3_{10} helical structure outlined in yellow and p21 μ peptide shown in olive green. Made using Pymol [19]. Crystallographic information can be found in Table S2 and Figures S2 and S4.

3.4. X-ray Crystallography Study of afumPCNA and p21 μ -afumRFC Reveals a Ring-like Structure

The co-crystal structure of afumPCNA bound with the p21 μ -afumRFC peptide was solved at a resolution of 2.30 Å in order to examine the structural features of an Afum-derived PIP-box (Figure 5a,b).

The KRRMP amino acids of the p21 μ -afumRFC peptide (Table 3) fold over the PIP-box, not interacting with the afumPCNA's surface (Figure 5c). This is caused by a change in the sequence of the PIP-box compared to the human RFC sequence (Table 3); the inclusion of a proline residue causes a kink, and the backbone carbonyl of ProXXX interacts with the Asp₁₄₇ backbone amide and Asn₁₅₀ residue side chain to stabilize the turn in the peptide (Figure 4c). The second arginine, Arg₁₄₃, is located close to the third arginine, Arg₁₄₉, producing a loop structure (143–149). The Met₁₄₄ side chain does not interact with the afumPCNA surface pocket as Gln₁₄₄ in the p21 μ PIP-box does with hPCNA. The Met₁₄₄ backbone amide does interact with the Asn₁₅₀ side chain and in turn also interacts with the Asp₁₄₇ side chain, supporting the 3_{10} helix via extra contacts that hold the compact structure (Figure 4c).

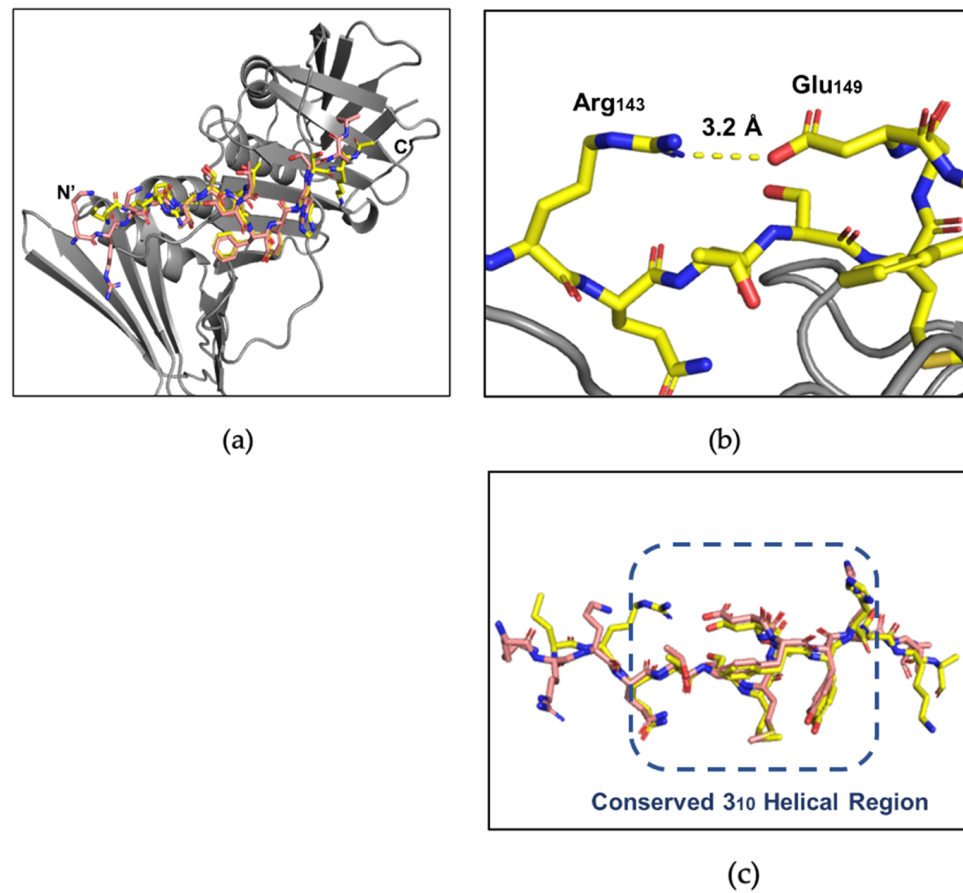


Figure 4. Comparison of the p21 μ peptide bound to hPCNA (PDB: 7KQ1) and p21 μ peptide bound to afumPCNA (PDB: 8GJF). (a) hPCNA shown in grey, p21 μ (PDB: 7KQ1) shown in salmon, and p21 μ (PDB: 8GJF) shown in yellow. (b) Arg₁₄₃ and Glu₁₄₉ salt bridge interaction in p21 μ (PDB: 8GJF) structure. (c) Conserved 3₁₀ helical and PIP-box region of p21 μ peptides, residues 144–152: p21 μ (PDB: 7KQ1) shown in salmon and p21 μ (PDB: 8GJF) shown in yellow (RMSD: 0.939 Å).

Table 3. Candidate fungal protein Peptide SPR data against afumPCNA. Peptide p21 μ afumRFC was also tested against human PCNA. Tested in triplicate. K_D is the affinity constant. SD, standard deviation. All peptides are C terminally amidated. Changes to the p21 μ scaffold are indicated in bold. More information can be found in Table S1.

Name	Sequence	afumPCNA Binding Affinity		Human PCNA Binding Affinity	
		K _D (nM) ± K _D SD (nM)		K _D (nM) ± K _D SD (nM)	
p21 μ afumDNALIG	¹⁴¹ KRRQ R VRSIASFFHSKR ¹⁵⁷	458 ± 117.77		-	
p21 μ afumDNAPOL	¹⁴¹ KRRQ K ELSRFDFFHSKR ¹⁵⁶	659.3 ± 105.8		-	
p21 μ afumFEN1	¹⁴¹ KRRQ S RLEGFFHSKR ¹⁵⁵	713 ± 56.9		-	
p21 μ afumRFC	¹⁴¹ KRRM P TDIRNFFHSKR ¹⁵⁶	94.84 ± 8.76		295 ± 6.9	

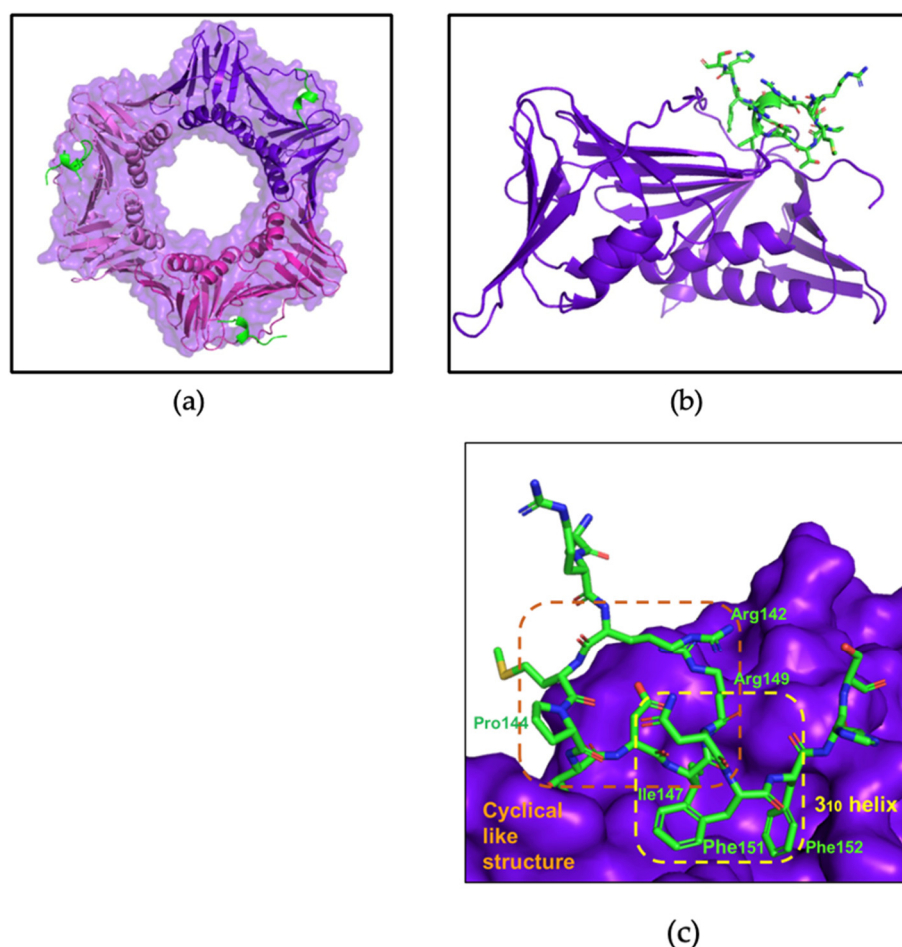


Figure 5. afumPCNA bound with p21 μ -afumRFC structure (PDB:8GJ5). (a) Trimer: afumPCNA surface shown in purple and p21 μ -afumRFC shown in green. (b) Monomer: afumPCNA shown in purple and p21 μ -afumRFC shown in green. (c) PIP-box binding site: 3₁₀ helical structure outlined in yellow and cyclical-like secondary structure outlined in orange. p21 μ -afumRFC peptide shown in green. Made using PyMOL [19]. Crystallographic information can be found in Table S2 and Figures S3 and S5.

4. Discussion

4.1. The p21 Peptide Library Interacts with afumPCNA with Similar Affinity and Structural Trends as hPCNA

The co-crystal structure of afumPCNA bound to the p21 μ peptide supports the hypothesis that *A. fumigatus* adopts a PIP-box sequence as a method for proteins to interact with afumPCNA.

The SPR (Table 1) results indicate that the binding of the p21 peptide library to afumPCNA generally follows the same trends seen in the hPCNA investigation [18]. This includes modifications at similar positions that cause similar changes in binding affinity across the two PCNA species.

It was previously hypothesized from results in molecular dynamics studies [14] that differences in the residues of the IDCL of afumPCNA and hPCNA could provide specificity for afumPCNA over hPCNA for a peptidomimetic inhibitor. However, this does not seem to be supported, as high-affinity peptidomimetic residues have a similar trend in affinity for hPCNA and afumPCNA. This is directly shown in the binding of rational design mutant 2 (RD2) to afumPCNA (Figure S6) [18], which was specifically designed for hPCNA, but it binds to the surface of afumPCNA with the same structure and a K_D of 20.3 nM (Table 1). The two PCNA species cannot be differentiated in specificity through the changes in PIP-box residues via the modifications investigated here.

4.2. Fungal Protein Replication Factor C PIP-Box Candidate Peptide Has a High Affinity for afumPCNA

Previously, a p21 peptide with the human RFC PIP-box, p21 μ -RFC, which has a seven-amino-acid PIP-box, MDIRKFF, was investigated to understand variations in the canonical sequence, and it was found to have a K_D value of 145 nM [18]. It was hypothesised here that this affinity was due to the position of residues Ile₁₄₇, Phe₁₅₀, and Phe₁₅₁, which form a hydrophobic three-pronged plug that inserts into the hydrophobic cleft of hPCNA [18]. Via computational modelling, it was observed that this would result in the extension of the arginine residue of position four over the conserved glutamine pocket in order to interact with hPCNA residue Val₄₅ [18].

The p21 μ -afumRFC PIP-box has an affinity for afumPCNA of less than 100 nM. This may be accounted for solely by the Ile₁₄₇, Phe₁₅₀, and Tyr₁₅₁ residues (Table 1), as previous research has shown these conserved residues to be highly favourable, especially Ile₁₄₇. The p21 μ -afumRFC PIP-box has a lower affinity for hPCNA than afumPCNA (Table 3). This is not only attributed to the lack of Gln₁₄₄, similarly to that of the human RFC peptide, but also the extra residues (Pro₁₄₅, Thr₁₄₆, and Asn₁₅₀) of the PIP-box for which the canonical positions do not exactly fit the conserved motif. It was hypothesised [18,35] that the Gln₁₄₄ residue was essential to the p21 peptide with respect to high-affinity binding; hence, it is present in p21 μ -RD2. The Gln₁₄₄ of p21 is known to contribute significantly to the binding affinity of hPCNA, as a Gln144Ala modification was not able to effectively inhibit DNA replication in vitro [18,35]. Gln₁₄₄ was considered at first to remain important in the Afum binding since the modification of p21 μ -Q144M decreases the binding affinity of the p21 μ -Q144M peptide to afumPCNA from 265.1 nM to 41.4 μ M. This is solely attributed to the single residue change as the secondary structure is maintained (Figure S7). However, here, its importance has still been questioned for the afumPCNA binding domain due to its absence in the candidate fungal RFC PIP-box. The attributes of p21 μ -afumRFC affinity for afumPCNA, although the canonical PIP-box is not followed, appear to be the unique secondary structure that is formed, which is discussed further.

4.3. The p21 μ afumRFC Peptide Has a Unique Structure That Could Be Exploited for an Antifungal Treatment

Peptidomimetic drug pipelines often reach the point of requiring a cell-permeable mechanism; a convenient method of improving cell uptake is via the cyclisation of the peptide. Cyclic peptides have been shown to enter the mammalian cell cytosol via multiple mechanisms, including passive diffusion, which is facilitated predominantly by hydrophobic side chains and small amino acid size (approximately 10 amino acids long), and endocytic uptake and endosomal escape [36].

In a structure such as the p21 PIP-box, which creates a 3_{10} helix, constraining this structure via cyclisation would allow the preorganization of the backbone and reduce the entropic cost of forming the secondary structure upon binding. Another advantage is that cyclical peptides may have improved cell permeability, which has been investigated in previous studies [37,38]. The investigation studied such macrocycles bound hPCNA with K_D values ranging from 570 nM to 3.86 μ M, with a bimane-constrained peptide proving to be the most potent. This peptide was also cell-permeable and localized to the cell cytosol of breast cancer cells (MDA-MB-468). The 3_{10} -helical structure was present in the computationally modelled structure. However, the analysis showed the peptide did not have a rigid 3_{10} helix in the solution when not bound to PCNA as NMR revealed it was not present in the solution [38]. This suggested that the pre-defining of a peptide backbone may not improve PCNA binding affinity. A 'linker' is a covalent tether that connects two distant parts of a peptide sequence to create a bridge and consequently preorganise the peptide backbone into a conformation that is suitable to bind to its target. It has been reported that a linker that affords flexibility in its cyclised structure may be preferable to enable the peptide to adopt its ideal conformation upon binding. This could be provided using the p21 μ afumRFC peptide by constraining the Arg₁₄₃ and Arg₁₄₉ residues as a linker to cyclise the peptide.

The p21 μ -afumRFC secondary structure looks as if it naturally mimics a ring such as that of the bimeane structure (Figure 6a). This could be used as a scaffold for a peptidomimetic, which could be improved to be fungal-cell-penetrable, as it has already been shown to not interfere with the 3_{10} helical turn upon binding. The two Arg residues can be replaced to create a linkage that, based on the X-ray crystallography structure, would not interrupt the 3_{10} -helical conformation and side chain exposure required for binding to afumPCNA, as these are 3.5 Å distance apart in the naturally forming architecture. The ability to outcompete afumPCNA's binding in the cell may be achieved via the incorporation of select p21 μ -RD2 mutant sequence residues in the p21 μ -afumRFC peptide, such as the combination of Tyr₁₅₀ and Phe₁₅₁ aromatic residues, which was shown to be essential in the affinity assay (Table 1).

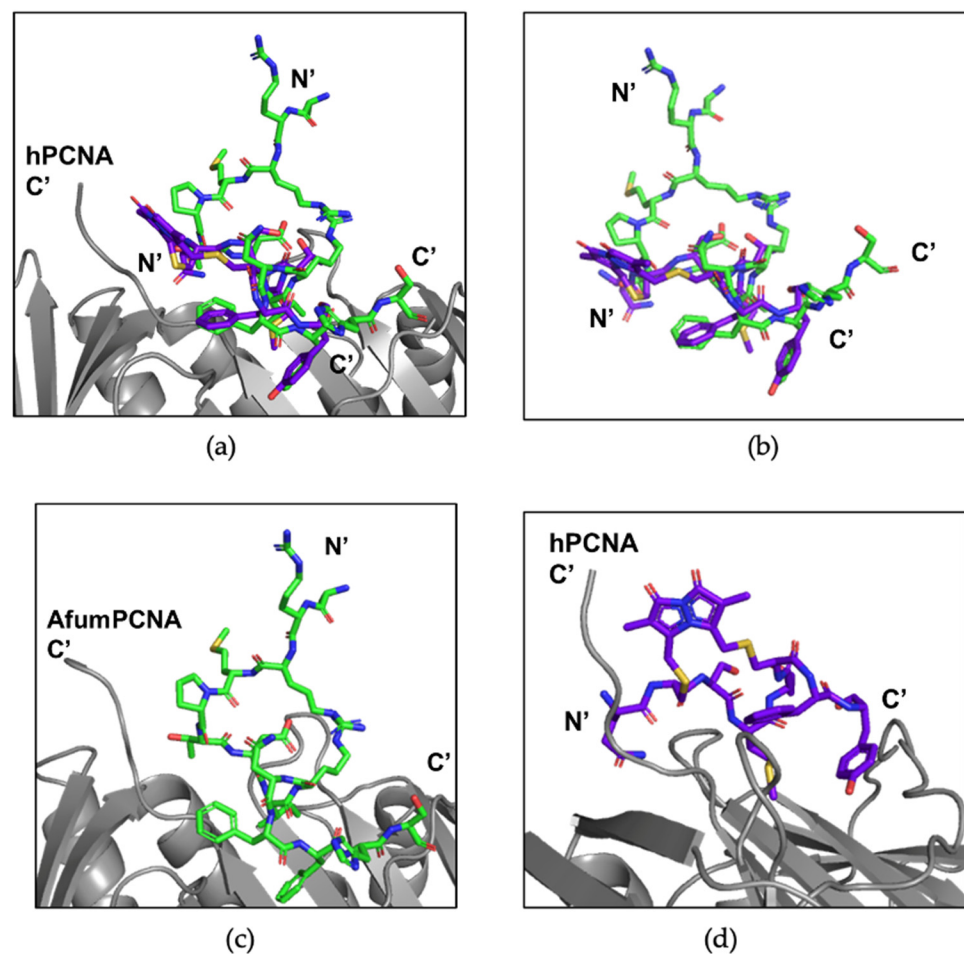


Figure 6. Previous p21-constrained peptides in comparison to the new p21 μ afumRFC peptide crystal structure. (a) p21 μ afumRFC peptide (green) crystal structure bound to the afumPCNA monomer (grey). p21 μ afumRFC peptide (green) produced an affinity of 295 ± 6.9 nM to hPCNA. (b) The Bimeane peptide (purple) docked to the hPCNA monomer (grey), as shown in the computational model, produced an affinity of 570 ± 30 nM to hPCNA [38]. (c) p21 μ afumRFC peptide (green) superimposed over the Bimeane peptide (purple) and hPCNA (grey) computational model. (d) p21 μ afumRFC peptide (green) superimposed over the Bimeane peptide (purple) computational model.

The bimeane peptide (Figure 6b,c) has a unique interaction in which the bimeane linker interacts with the C-terminal end of PCNA. This is also achieved in the RFC peptide via the interaction of the proline residue interacting with the C-terminal end of afumPCNA. The key difference in the scaffolds is that the RFC peptide also carried out interactions on the other side of the PIP-box binding domain through the Arg₁₄₉ side chain. This is believed to

achieve a more ideal surface packing of the PIP-box onto afumPCNA than previous cyclical peptides have achieved.

Adding a cell-penetrating peptide (CPP) or fungal-specific peptide to the N- or C-terminus of this structure would, based on the X-ray crystallographic structure, not interfere with PIP-box binding and the secondary structure, a problem found for other investigated linkers incorporated into p21 PIP-box peptides. Although high levels of translocation were typically associated with the toxicity of peptides towards fungal cells, SynB, an 18-amino-acid-long peptide, has been found in previous studies of CPPs to be specific for fungal cells with respect to efficiently translocating into the human fungal pathogen *Candida albicans* at concentrations that led to minimal toxicity [39]. Lowered toxicity is vital for experimental studies in assessing the specification of afumPCNA inhibition over fungal cell toxicity.

5. Conclusions

Here, we present the first structure of a p21 PIP-box peptide bound to *A. fumigatus* PCNA, as well as fungal PIP-box candidates, demonstrating the hypothesis that the fungal replication model uses a PIP-box sequence as a method for binding to fungal PCNA.

A high-affinity rational design for a potential cell-permeable peptidomimetic is presented via the combination of a cyclised structure of the p21 μ afumRFC peptide. Via full cyclisation and the incorporation of select p21 μ -RD2 mutant sequence residues, this peptide could be used in the next stages of the drug discovery pipeline as a potential fungal therapeutic. This could be carried out via the addition of a linker to the cyclized secondary structure. Future work will focus on specific fungal cell permeability via the utilisation of the N-terminus of the peptide, which makes no contact with the surface of PCNA and cannot interfere with the helical and cyclized 3₁₀ structure.

Supplementary Materials: The following supporting information can be downloaded at <https://www.mdpi.com/article/10.3390/jof9111098/s1>.

Author Contributions: B.C.V. is responsible for conceptualization, methodology, formal analysis, investigation, writing—original draft preparation, and review and editing final. A.J.H. is responsible for resources, investigation, and methodology. J.L.P. is responsible for intellectual support, review and editing. J.B.B. is responsible for resources, writing—review and editing visualization, supervision, project administration, and funding. A.D.A. is responsible for supervision and resources. All authors have read and agreed to the published version of the manuscript.

Funding: This research received no external funding.

Institutional Review Board Statement: Not applicable.

Informed Consent Statement: Not applicable.

Data Availability Statement: Data are contained within the article or Supplementary Materials. The data presented in this study are available in Supplementary Materials.

Acknowledgments: B. Vandborg and A. Horsfall and J. Pederick were supported by an Australian Government Research Training Program stipend scholarship. This research was undertaken in part using the MX1 and MX2 beamlines at the Australian Synchrotron and part of ANSTO and made use of the Australian Cancer Research Foundation detector. Special thanks are given to William Walters, Paul Jr Walters, and Polly Walters for their crystallography consultation. Special thanks are given to Jakeb Vandborg for their scientific consultation.

Conflicts of Interest: The authors declare no conflict of interest.

References

1. Bitar, D.; Lortholary, O.; Le Strat, Y.; Nicolau, J.; Coignard, B.; Tattevin, P.; Che, D.; Dromer, F. Population-based analysis of invasive fungal infections, France, 2001–2010. *Emerg. Infect. Dis.* **2014**, *20*, 1149–1155. [[CrossRef](#)]
2. McNeil, M.; Nash, S.L.; Hajjeh, R.A.; Phelan, M.A.; Conn, L.A.; Plikaytis, B.D.; Warnock, D.W. Trends in mortality due to invasive mycotic diseases in the United States, 1980–1997. *Clin. Infect. Dis.* **2001**, *33*, 641–647. [[CrossRef](#)]
3. Latgé, J.-P.; Chamilos, G. *Aspergillus fumigatus* and Aspergillosis in 2019. *Clin. Microbiol. Rev.* **2019**, *33*, 00140–18. [[CrossRef](#)]

4. Rhodes, J.; Abdolrasouli, A.; Dunne, K.; Sewell, T.R.; Zhang, Y.; Ballard, E.; Brackin, A.P.; van Rhijn, N.; Chown, H.; Tsitsopoulou, A.; et al. Population genomics confirms acquisition of drug-resistant *Aspergillus fumigatus* infection by humans from the environment. *Nat. Microbiol.* **2022**, *7*, 663–674. [[CrossRef](#)]
5. Yoon, H.; Choi, H.Y.; Kim, Y.K.; Song, Y.J.; Ki, M. Prevalence of fungal infections using National Health Insurance data from 2009–2013, South Korea. *Epidemiol. Health* **2014**, *36*, e2014017. [[CrossRef](#)]
6. Van de Veerndonk, F.L.; Gresnigt, M.S.; Romani, L.; Netea, M.G.; Latgé, J.-P. *Aspergillus fumigatus* morphology and dynamic host interactions. *Nat. Rev. Microbiol.* **2017**, *15*, 661–674. [[CrossRef](#)]
7. Gallien, S.; Fournier, S.; Porcher, R.; Bottero, J.; Ribaud, P.; Sulahian, A.; Molina, J.M. Therapeutic outcome and prognostic factors of invasive aspergillosis in an infectious disease department: A review of 34 cases. *Infection* **2008**, *36*, 533–538. [[CrossRef](#)]
8. Sugui, J.; Kwon-Chung, K.J.; Juvvadi, P.R.; Latge, J.P.; Steinbach, W.J. *Aspergillus fumigatus* and related species. *Cold Spring Harb Perspect. Med.* **2015**, *5*, a019786. [[CrossRef](#)]
9. Steinbach, W. Are we there yet? Recent progress in the molecular diagnosis and novel antifungal targeting of *Aspergillus fumigatus* and invasive aspergillosis. *PLoS Pathog.* **2013**, *9*, e1003642. [[CrossRef](#)]
10. Arastehfar, A.; Carvalho, A.; Houbraken, J.; Lombardi, L.; Garcia-Rubio, R.; Jenks, J.D.; Rivero-Menendez, O.; Aljohani, R.; Jacobsen, I.D.; Berman, J.; et al. *Aspergillus fumigatus* and aspergillosis: From basics to clinics. *Stud. Mycol.* **2021**, *100*, 100115. [[CrossRef](#)]
11. Ben-Ami, R.; Lewis, R.E.; Kontoyiannis, D.P. Enemy of the (immunosuppressed) state: An update on the pathogenesis of *Aspergillus fumigatus* infection. *Br. J. Haematol.* **2010**, *150*, 406–417. [[CrossRef](#)]
12. Resendiz Sharpe, A.; Lagrou, K.; Meis, J.F.; Chowdhary, A.; Lockhart, S.R.; Verweij, P.E.; ISHAM/ECMM *Aspergillus* Resistance Surveillance Working Group. Triazole resistance surveillance in *Aspergillus fumigatus*. *Med. Mycol.* **2018**, *56*, S83–S92. [[CrossRef](#)] [[PubMed](#)]
13. Edouarzin, E.; Horn, C.; Paudyal, A.; Zhang, C.; Lu, J.; Tong, Z.; Giaever, G.; Nislow, C.; Veerapandian, R.; Hua, D.H.; et al. Broad-spectrum antifungal activities and mechanism of drimane sesquiterpenoids. *Microb. Cell* **2020**, *7*, 146–159. [[CrossRef](#)]
14. Marshall, A.C.; Kroker, A.J.; Murray, L.A.; Gronthos, K.; Rajapaksha, H.; Wegener, K.L.; Bruning, J.B. Structure of the sliding clamp from the fungal pathogen *Aspergillus fumigatus* (AfumPCNA) and interactions with human p21. *FEBS J.* **2017**, *284*, 985–1002. [[CrossRef](#)] [[PubMed](#)]
15. Maga, G.; Hubscher, U. Proliferating cell nuclear antigen (PCNA): A dancer with many partners. *J. Cell Sci.* **2003**, *116*, 3051–3060. [[CrossRef](#)]
16. Sakakura, C.; Hagiwara, A.; Tsujimoto, H.; Ozaki, K.; Sakakibara, T.; Oyama, T.; Takahashi, T. The anti-proliferative effect of proliferating cell nuclear antigen-specific antisense oligonucleotides on human gastric cancer cell lines. *Surg. Today* **1995**, *25*, 184–186. [[CrossRef](#)] [[PubMed](#)]
17. Naryzhny, S.; Lee, H. Characterization of proliferating cell nuclear antigen (PCNA) isoforms in normal and cancer cells: There is no cancer-associated form of PCNA. *FEBS Lett.* **2007**, *528*, 4917–4920. [[CrossRef](#)] [[PubMed](#)]
18. Horsfall, A.J.; Vandborg, B.A.; Kowalczyk, W.; Chav, T.; Scanlon, D.B.; Abell, A.D.; Bruning, J.B. Unlocking the PIP-box: A peptide library reveals interactions that drive high-affinity binding to human PCNA. *J. Biol. Chem.* **2021**, *296*, 100773. [[CrossRef](#)]
19. Schrodinger LLC. *The PyMOL Molecular Graphics System*, Version 1.2r3pre; Schrodinger LLC: New York, NY, USA, 2015.
20. Warbrick, E. PCNA binding through a conserved motif. *Bioessays* **1998**, *20*, 195–199. [[CrossRef](#)]
21. Gulbis, J.M.; Kelman, Z.; Hurwitz, J.; O'Donnell, M.; Kuriyan, J. Structure of the C terminal region of p21(WAF1/CIP1) complexed with human PCNA. *Cell* **1996**, *87*, 297–306. [[CrossRef](#)]
22. Prestel, A.; Wichmann, N.; Martins, J.M.; Marabini, R.; Kassem, N.; Broendum, S.S.; Otterlei, M.; Nielsen, O.; Willemoes, M.; Ploug, M.; et al. The PCNA interaction motifs revisited: Thinking outside the PIP-box. *Cell. Mol. Life Sci.* **2019**, *76*, 4923–4943. [[CrossRef](#)] [[PubMed](#)]
23. Vandborg, B.; Holroyd, D.L.; Pukala, T.; Bruning, J.B. Production of recombinant human proliferating cellular nuclear antigen (PCNA) for structural and biophysical characterization. *Protein Expr. Purif.* **2023**, *212*, 106353. [[CrossRef](#)] [[PubMed](#)]
24. Anthis, N.J.; Clore, G.M. Sequence-specific determination of protein and peptide concentrations by absorbance at 205 nm. *Protein Sci.* **2013**, *22*, 851–858. [[CrossRef](#)]
25. Kabsch, W. XDS (X-ray detector software). *Acta Crystallogr. D Biol. Crystallogr.* **2010**, *66*, 125–132. [[CrossRef](#)] [[PubMed](#)]
26. Winn, M.D.; Ballard, C.C.; Cowtan, K.D.; Dodson, E.J.; Emsley, P.; Evans, P.R.; Keegan, R.M.; Krissinel, E.B.; Leslie, A.G.W.; McCoy, A.; et al. Overview of the CCP4 suite and current developments. *Acta Crystallogr. D Biol. Crystallogr.* **2011**, *67*, 235–242. [[CrossRef](#)]
27. Potterton, E.; Briggs, P.J.; Turkenburg, M.G.W.; Dodson, E. A graphical user interface to the CCP4 program suite. *Acta Crystallogr. D Biol. Crystallogr.* **2003**, *59*, 1131–1137. [[CrossRef](#)]
28. McCoy, A.J.; Grosse-Kunstleve, R.W.; Adams, P.D.; Winn, M.D.; Storonia, L.C.; Read, R.J. Phaser crystallographic software. *J. Appl. Crystallogr.* **2007**, *40*, 658–674. [[CrossRef](#)]
29. Afonine, P.V.; Grosse-Kunstleve, R.W.; Echols, N.; Headd, J.J.; Moriarty, N.W.; Mustyakimov, M.; Terwilliger, T.C.; Urzhumtsev, A.; Zwart, P.H.; Adams, P.D. Towards automated crystallographic structure refinement with phenix.refine. *Acta Crystallogr. D Biol. Crystallogr.* **2012**, *68*, 352–367. [[CrossRef](#)]
30. Liebschner, D.; Afonine, P.V.; Baker, M.L.; Bunkóczi, G.; Chen, V.B.; Croll, T.I.; Hintze, B.; Hung, L.W.; Jain, S.; McCoy, A.J.; et al. Phenix: Macromolecular structure determination using X-rays, neutrons and electrons: Recent developments in phenix. *Acta Crystallogr. D Biol. Crystallogr.* **2019**, *75*, 861–877. [[CrossRef](#)]

31. Emsley, P.; Cowtan, K. Coot: Model-building tools for molecular graphics. *Acta Crystallogr. D Biol. Crystallogr.* **2004**, *60*, 2126–2132. [[CrossRef](#)]
32. Abagyan, R.; Totrov, M. Biased probability Monte Carlo conformational searches and electrostatic calculations for peptides and proteins. *J. Mol. Biol.* **1994**, *235*, 983–1002. [[CrossRef](#)] [[PubMed](#)]
33. Abagyan, R.; Totrov, M.; Kuznetsov, D. ICM—A new method for protein modeling and design: Applications to docking and structure prediction from the distorted native conformation. *J. Comput. Chem.* **1994**, *15*, 488–506. [[CrossRef](#)]
34. Horsfall, A.; Abell, A.; Bruning, J. Targeting PCNA with peptide mimetics for therapeutic purposes. *ChemBioChem* **2019**, *21*, 442–450. [[CrossRef](#)]
35. Boehm, E.; Washington, M.T. R.I.P. to the PIP: PCNA-binding motif no longer considered specific. *BioEssays* **2016**, *38*, 1117–1122. [[CrossRef](#)] [[PubMed](#)]
36. Dougherty, P.G.; Ashweta, S.; Dehua, P. Understanding Cell Penetration of Cyclic Peptides. *Chem. Rev.* **2019**, *119*, 10241–10287. [[CrossRef](#)] [[PubMed](#)]
37. Wegener, K.L.; McGrath Amy, E.; Dixon Nicholas, E.; Oakley Aaron, J.; Scanlon Denis, B.; Abell Andrew, D.; Bruning John, B. Rational Design of a 310 -Helical PIP-Box Mimetic Targeting hPCNA, the Human Sliding Clamp. *Eur. J. Chem.* **2018**, *24*, 11325–11331. [[CrossRef](#)]
38. Horsfall, A.J.; Vandborg, B.A.; Kikhtyak, Z.; Scanlon, D.B.; Tilley, W.D.; Hickey, T.E.; Bruning, J.B.; Abell, A.D. A cell permeable bimane-constrained PCNA-interacting peptide. *RSC Chem. Biol.* **2021**, *2*, 1499–1508. [[CrossRef](#)]
39. Gong, Z.; Karlsson, A.J. Translocation of cell-penetrating peptides into *Candida* fungal pathogens. *Protein Sci.* **2017**, *26*, 1714–1725. [[CrossRef](#)]

Disclaimer/Publisher’s Note: The statements, opinions and data contained in all publications are solely those of the individual author(s) and contributor(s) and not of MDPI and/or the editor(s). MDPI and/or the editor(s) disclaim responsibility for any injury to people or property resulting from any ideas, methods, instructions or products referred to in the content.